

## THERMAL ANALYSIS OF FRICTION STIR WELDING USING TOOLS WITH VARYING SHOULDER SIZES

Diksha Patil<sup>1</sup>, Vineet Kumar Dwivedi<sup>2</sup>

<sup>1</sup>Scholar, School of Mechanical Engineering, Faculty of Engineering and Technology, SAM Global University, Bhopal, M.P, 462022, India.

<sup>2</sup>Head and Prof., School of Mechanical Engineering, Faculty of Engineering and Technology, SAM Global University, Bhopal, M.P, 462022, India.

### ABSTRACT

This study investigates the effects of shoulder size on the thermal distribution in friction stir welding (FSW) using computational simulations. By modeling shoulder diameters of 26 mm, 34 mm, 42 mm, and 50 mm, the research explores how variations in shoulder size impact temperature profiles and heat distribution within the workpiece. Results reveal that larger shoulder diameters significantly increase peak temperatures and extend the heated zone due to enhanced frictional heating at the shoulder-workpiece interface. The temperature gradient is observed to be steeper ahead of the tool than behind it, attributed to heat accumulation and reduced diffusivity in the trailing region. This asymmetry indicates that shoulder size affects both maximum temperature and heat dissipation rates, with larger diameters intensifying the overall thermal effect. The study emphasizes that shoulder diameter optimization is crucial for controlling the thermal profile in FSW, which has implications for the mechanical properties and integrity of welded joints. These findings provide a foundation for enhancing FSW parameters to achieve improved weld quality in industrial applications.

**Keywords:** Friction Stir Welding, Shoulder Diameter, Thermal Analysis, Temperature Distribution, Computational Simulation

### 1. INTRODUCTION

Friction Stir Welding (FSW), a solid-state joining process, has emerged as a highly effective method for welding lightweight materials, such as aluminum alloys, often used in aerospace, automotive, and marine applications. Unlike traditional welding, FSW produces a joint by mechanically stirring the workpieces with a rotating, non-consumable tool, leading to lower residual stresses, minimal distortion, and enhanced mechanical properties. The tool design, particularly the pin profile, is critical in influencing the heat generation and material flow during FSW, which directly impacts the weld quality and thermal characteristics of the process. The thermal behavior in FSW is a key factor that governs the microstructural evolution, mechanical properties, and defect formation in the weld zone. Heat generation during the process depends on several parameters, including the tool rotation speed, traverse speed, and, notably, the pin profile. Different pin geometries, such as cylindrical, tapered, and threaded designs, alter the contact surface area and material interaction, influencing the temperature distribution in the weld zone. This paper focuses on analyzing the thermal effects induced by varying pin profiles during FSW, aiming to optimize tool design for improved weld quality. By examining the influence of different pin profiles on heat generation and distribution, this study seeks to deepen the understanding of thermal mechanisms in FSW and contribute to the development of more efficient, high-quality joining techniques for advanced engineering applications.

J. V. Christy et al. [1] discuss the difficulties associated with fusion welding aluminum alloys, highlighting issues like porosity and solidification cracking. They examine alternative techniques, such as underwater friction stir welding (UFSW) and vibrational friction stir welding (VFSW), with a particular focus on VFSW for its potential in energy savings and adaptability. The authors also recommend further research on friction stir welding for aluminum matrix composites (Al-MMCs). C. Zhang et al. [2] analyzed dissimilar joints of AA2024-T351 and AA7075-T651 formed through friction stir welding (FSW) with high heat input, examining how post-weld heat treatment (PWHT) impacts their microstructure and mechanical characteristics. The study observed abnormal grain growth (AGG) in the nugget zone (NZ) after PWHT, contrasting with the fine equiaxed grains present in the as-welded joint. Grain growth was more pronounced on the AA2024 side, and the joint performance showed no improvement post-PWHT, as fractures occurred in the NZ due to weak interface penetration. P. Kah et al. [3] highlight the transportation industry's need for energy-efficient, sustainable solutions, noting aluminum alloys' critical role due to their lightweight properties. Although advancements in aluminum welding techniques have addressed several challenges, defects remain. The study examines defect formation in friction stir welding, laser welding, and arc welding of aluminum, exploring the relationship between FSW parameters and weld defects, as well as issues like porosity and hot cracking in laser welding. It also covers metallurgical factors affecting microstructure and defect mitigation in arc welding. K. R. Ramkumar et al. [4] examined AA7075/TiC metal matrix composites (MMCs) fabricated through stir casting, with varying TiC content (0, 2.5, 5, and

7.5 wt.%). They used X-ray diffraction and electron microscopy to characterize the composites and evaluated mechanical properties, such as flexural strength and hardness, and tribological properties, like wear resistance and friction coefficient. The study found that TiC dispersion significantly improved mechanical and surface properties compared to AA7075, confirming successful composite formation without intermetallic phases and demonstrating TiC's beneficial effect on AA7075. C. Zhang et al. [5] investigated the influence of rotational speed on the microstructure, mechanical properties, and corrosion resistance of dissimilar FSW AA2024/7075 joints. Results showed that rotational speed affected the local microstructure, creating fine equiaxed grains in the NZ, with grain size decreasing from the shoulder to the bottom. The study achieved optimal tensile strength (411.4 MPa) at 950 rpm, representing 87.6% welding efficiency relative to AA2024. Corrosion resistance was highest at this rotational speed due to optimal precipitate characteristics. Y. C. Chen et al. [6] studied precipitate evolution in FSW 2219-T6 aluminum alloys using transmission electron microscopy. In the weld nugget zone (WNZ) and thermo-mechanically affected zone (TMAZ), certain metastable precipitates transformed into stable phases, while others dissolved into the aluminum matrix. In the heat-affected zone (HAZ), the thermal and mechanical effects of welding led to precipitate coarsening, resulting in notable microstructural changes. S. Raja et al. [7] reviewed the emerging application of nanomaterial reinforcement in FSW to improve joint properties, enhancing characteristics like hardness, strength, corrosion resistance, wear resistance, and fatigue life. The review discusses nanoparticle types, their properties, and behavior in FSW, as well as the methods used for nanoparticle deposition. It also analyzes the microstructural changes brought about by reinforcement and concludes with potential future developments in this area. J. Li et al. [8] examined the FSW of 7A04-T6 aluminum alloys, achieving the highest tensile strength at a welding speed of 120 mm/min and rotation speed of 1000 r/min, reaching 77.93% of the base material's strength. Fine grains in the nugget zone (NZ) hindered crack propagation, enhancing joint toughness. Fatigue testing showed decreasing fatigue strength with increasing fatigue life, and fractures occurred in the HAZ. A post-weld laser heat treatment further refined the microstructure, improving mechanical properties. A. Heiderazadeh et al. [9] explored how FSW and friction stir processing (FSP) affect microstructure and performance by inducing large strains, high temperatures, and high strain rates. While most studies focus on optimizing FSW parameters, this study emphasizes understanding microstructural evolution, including grain structure development, phase transformations, and precipitation across various materials, especially in dissimilar metal joints. The review also highlights FSP's role in localized microstructure refinement and the formation of metal matrix composites, identifying knowledge gaps and suggesting directions for future research. R. Kesharwani et al. [10] examined the microstructure, mechanical properties, and texture evolution of AA6061-T6 MMCs reinforced with silicon carbide (SiC) and zinc (Zn) particles through FSW. The stirred zone (SZ) showed significant grain refinement, with SiC and Zn particle-reinforced composites exhibiting textures like P {011} <112>, cube {001} <101>, copper {112} <111>, and Goss {110}. The SiC composite had a microhardness of  $110 \pm 4$  HV0.2, while the Zn composite reached  $120 \pm 5$  HV0.2, with tensile strengths of 224 MPa and 236 MPa, respectively.

### 1.1 Scope of the Research

The shape and positioning of the pin in friction stir welding (FSW) play a crucial role in determining the welded joint's microstructure and mechanical properties by affecting thermal behavior and material flow. Experimental approaches face difficulties in tracking thermal characteristics accurately, as the rotating tool's movement complicates monitoring the temperature distribution and thermal history within the workpiece. Computational modeling provides an effective alternative, enabling thermal analysis across a wider range of geometric variables, thereby improving the depth and realism of thermal insights. Thermal Diagnostics with Polygonal Pins: To accurately estimate heat generation for various polygonal pin shapes, custom approaches are necessary. Computational Fluid Dynamics (CFD) models have been proposed to provide detailed thermal field analyses for these pin geometries. Thermal Diagnostics with Eccentric Polygonal Pins: Analyzing heat generation and thermal effects for eccentric polygonal pins is essential, as variations in pin position relative to the rotation axis alter the thermal distribution. Thermal Analysis with Tapered Eccentric Polygonal Pins: Differences in the pin's surface area impact heat generation, necessitating specialized estimation methods. The effect of taper severity on the welding thermal cycle also requires detailed examination.

### 1.2 Objective of the Study

- To develop a more realistic CFD model to simulate FSW process.
- To establish the effects of geometrical and operational parameters of FSW with polygonal pins on the temperature distribution and peak temperature within the workpiece.
- To determine the effects of geometrical and operational parameters of FSW using eccentric polygonal pins on the temperature distribution and peak temperature within the workpiece.

## 2. CFD MODELLING OF FRICTION STIR WEILDING

This section discusses the application of advanced Computational Fluid Dynamics (CFD) to simulate the thermal cycle in friction stir welding (FSW), aiming to enhance the realism of the model. By reducing assumptions, the study aims to bridge the gaps between simulations and real-world conditions. A three-dimensional, transient model of limited fluid regions was created using ANSYS Fluent 17.0, incorporating realistic tool translational motion. The methodology encompasses geometric modeling, mesh generation, solver configurations, and boundary conditions. Validation of the model involved comparing the simulation results with available experimental data, which demonstrated the model's accuracy in representing the thermal characteristics associated with FSW.

Method and analysis which is performed in your research work should be written in this section. A simple strategy to follow is to use keywords from your title in first few sentences.

### 2.1 The Governing Equation

CFD uses numerical methods to analyse the systems involving the fluid flow and the heat transfer and that basically depends on the governing equations of the fluid flow in their continuum forms. Therefore, the material flow in FSW is governed by mass and momentum conservation equations, while to describe the heat transfer process, energy conservation equation is used. In these equations the mathematical statements of the conservation laws of physics are represented. The continuity equation is given by

For a compressible fluid:

$$\partial\rho/\partial t + \partial(\rho u)/\partial x + \partial(\rho v)/\partial y + \partial(\rho w)/\partial z = 0$$

For an incompressible fluid:

$$\partial u/\partial x + \partial v/\partial y + \partial w/\partial z = 0$$

where  $u$ ,  $v$ , and  $z$  are the velocities in  $x$ ,  $y$ , and  $z$  directions, respectively. While, Navier-Stokes equation governs the momentum conservation in  $x$ ,  $y$ , and  $z$  directions:

Vector form of Navier-Stokes equation:

$$\rho (\partial u/\partial t + (u \cdot \nabla) u) = -\nabla p + \mu \nabla^2 u + f$$

where:

- $\rho$  = fluid density
- $u$  = velocity vector (with components  $u$ ,  $v$ ,  $w$  in  $x$ ,  $y$ , and  $z$  directions)
- $t$  = time
- $p$  = pressure
- $\mu$  = dynamic viscosity
- $\nabla^2 u$  = Laplacian of the velocity (representing viscous forces)
- $f$  = body force per unit volume (e.g., gravity)

Component form of Navier-Stokes equations:

For the  $x$ -direction:

$$\rho (\partial u/\partial t + u \partial u/\partial x + v \partial u/\partial y + w \partial u/\partial z) = -\partial p/\partial x + \mu (\partial^2 u/\partial x^2 + \partial^2 u/\partial y^2 + \partial^2 u/\partial z^2) + f_x$$

For the  $y$ -direction:

$$\rho (\partial v/\partial t + u \partial v/\partial x + v \partial v/\partial y + w \partial v/\partial z) = -\partial p/\partial y + \mu (\partial^2 v/\partial x^2 + \partial^2 v/\partial y^2 + \partial^2 v/\partial z^2) + f_y$$

For the  $z$ -direction:

$$\rho (\partial w/\partial t + u \partial w/\partial x + v \partial w/\partial y + w \partial w/\partial z) = -\partial p/\partial z + \mu (\partial^2 w/\partial x^2 + \partial^2 w/\partial y^2 + \partial^2 w/\partial z^2) + f_z$$

The energy conservation equation is written as:

$$\rho c_p (\partial T/\partial t + u \partial T/\partial x + v \partial T/\partial y + w \partial T/\partial z) = k (\partial^2 T/\partial x^2 + \partial^2 T/\partial y^2 + \partial^2 T/\partial z^2)$$

where:

- $\rho$  = fluid density
- $c_p$  = specific heat capacity at constant pressure
- $T$  = temperature
- $t$  = time
- $u$ ,  $v$ ,  $w$  = velocity components in the  $x$ ,  $y$ , and  $z$  directions, respectively
- $k$  = thermal conductivity

where  $T$  is the temperature,  $cp$  is the specific heat, and  $k$  is the thermal conductivity. By using the finite volume method, the governing equations for 3-D transient heat transfer and material flow are discretized and solved using ANSYS/FLUENT 17.0. For those who are interested in the numerical solutions of such engineering problems, different related titles are recommended here which present wide areas to discuss the treatment of incompressible, compressible and viscous flows as well as heat transfer problems.

## 2.2 Models Regions and Geometry

Using the Design Modeller facility in Ansys 17.0, the geometric details of the model have been created. As it can be seen in figure 3.1, the current numerical model has two main regions; the first one represents the thermomechanical affected zone (TMAZ) around the tool. This zone is treated as a fluid region which has a conical shape where, its dimensions are estimated based on design variables “ $x_1$ ” and “ $x_2$ ” as displayed in figure 3.2. The dimensions of this rotational zone “ $x_1$ ” and “ $x_2$ ” are 1mm and 2.5mm, respectively. The second region represents the other part of the workpiece which is treated as a solid region.

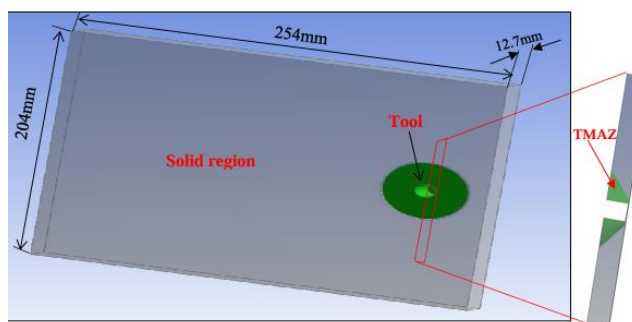


Figure 1: The main regions in the computation domain

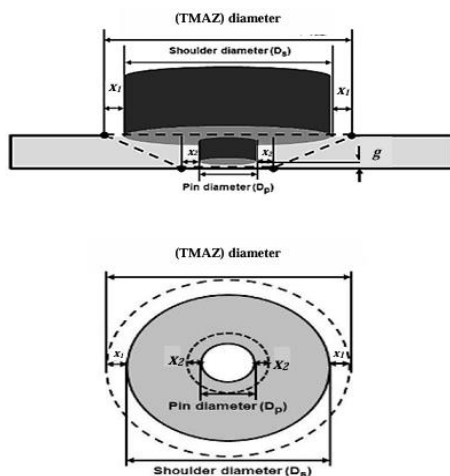


Figure 2: TMAZ details

Based on practical dimensions the numerical model of the computational domain consists of volumes of two plates of aluminium alloy AA6061, in contact with each other. The tool, consisting of the shoulder and the pin is being inserted into the workpiece at the interface of the two plates. The tool pin has a cylindrical profile with a radius of 6mm and a length of 12.0mm, where the shoulder has a constant radius of 25mm. The tool was simulated as a wall after cutting its material volume from the workpiece. The dimensions of each plate to be welded are 254mm x 102mm x 12.7mm.

The mesh quality and the minimization of element numbers were carefully optimized during the meshing of the computational domain. Given the study's goal of achieving a highly realistic model, the motion of the tool was also considered in selecting meshing techniques. The tool's rotation in the Thermo-Mechanically Affected Zone (TMAZ) was defined using the sliding mesh technique, as it accurately represents the moving tool's profile without approximations. Generally, temperature gradients diminish with increasing distance from the tool, but a sharp gradient exists close to the tool. To capture this detail, the TMAZ region was finely meshed. Considering the geometries of both the tool and workpiece, tetrahedral elements were chosen for meshing due to their ease of creation and acceptable skewness, reaching around 700,000 elements in total. Skewness, an indicator of mesh quality, recorded a value of 0.62, indicating good quality as high skewness values (above 0.95) are not recommended per ANSYS guidelines. Figure 3.3 shows the meshed computational domain with two cross-sections to illustrate the different zones and gradual meshing. Notably, the mesh shown is the initial mesh to be used during the dwelling stage of the welding process, where the tool undergoes only rotational motion.

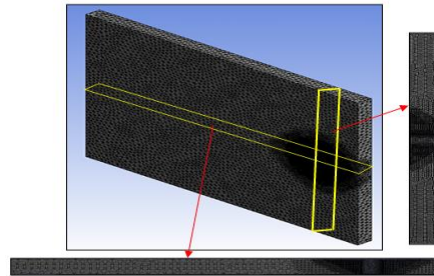


Figure 3: Meshing of the Computation Domain

### 3. THERMAL CHARACTERISATION OF FRICTION STIR WELDING USING TOOL WITH POLYGONAL PINS

To enhance understanding of the thermal dynamics in friction stir welding (FSW), this chapter outlines the use of the proposed CFD methodology to analyze the thermal field produced during FSW with polygonal pin tools. It examines how various geometric and operational parameters affect temperature distribution and peak temperature in a thick FS welded workpiece. Additionally, based on these findings, a semi-empirical model has been developed to predict peak temperatures more accurately.

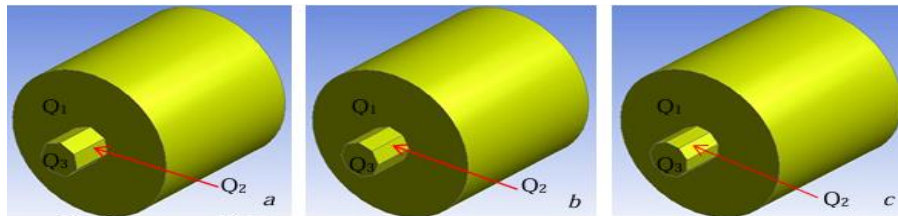


Figure 4: Tools with different pin profiles (a) Heptagon, (b) Octagon, (c) Nonagon.

To visualize the effect of shoulder diameter on the thermal field in friction stir welding, four diameters—26 mm, 34 mm, 42 mm, and 50 mm—were evaluated. The temperature distribution within the workpiece was monitored to determine the global maximum temperature. To demonstrate the changes in temperature profile over the 100-second welding cycle, shoulder diameters of 26 mm and 50 mm were analyzed at various time intervals. Figure 4.5 presents temperature contours on a vertical plane at the weld centerline, showcasing both the dwelling and welding phases. The temperature distribution along the pin length reveals a distinct trend: the lowest temperatures are found at the tip of the pin, with temperatures increasing towards the shoulder base. This pattern can be attributed to two main factors. Firstly, heat generation at the pin tip is lower due to its smaller frictional area. Secondly, the greatest heat generation occurs near the shoulder-workpiece interface, located near the top of the pin. The figure also indicates that the maximum temperature reached with a 50 mm shoulder diameter is significantly higher than that with a 26 mm diameter, which is linked to the larger frictional area associated with the increased shoulder size. In terms of process time, the initial temperature distribution shows high heating rates within the material. During the early dwelling period, maximum temperatures recorded at 1 second, 3 seconds, and 5 seconds were 578.6 K, 750.9 K, and 815.3 K, respectively, for a 25 mm shoulder radius. At 40 seconds, as the tool had shifted to a different position, the temperature rose to 836.1 K.

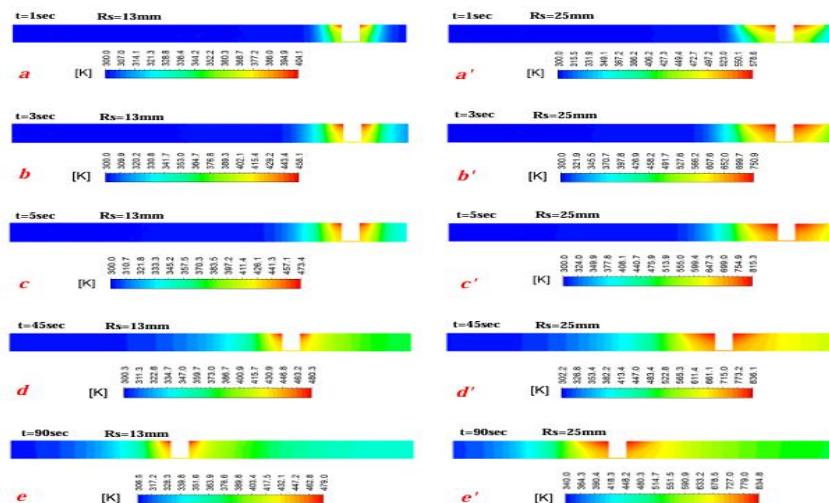
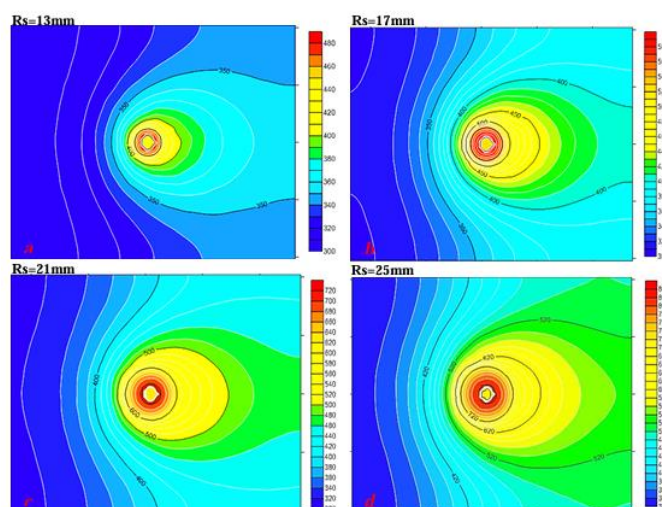


Figure 5: Temperature distribution vertical plane at different time steps calculated for shoulder diameters of 26mm and 50mm

To examine the impact of shoulder size on temperature distribution, snapshots were taken on the plane where the maximum temperature is expected. This plane covers the contact region between the shoulder and the workpiece, anticipated to display the global peak temperature. Given that frictional heating at this interface is the primary heat source, Figure (a, b, c, d) illustrates the hottest area concentrated around the tool. While the high-temperature contours surrounding the tool are almost symmetrically arranged, the temperature gradient is steeper in front of the tool than behind it. This asymmetry likely arises from reduced material diffusivity due to heat buildup behind the tool, leading to slower heat dissipation. Conversely, in the leading region, where parts of the workpiece remain at room temperature, the temperature profile indicates rapid heat dissipation. In Figure 6, with a shoulder radius of 25 mm, the minimum temperature is recorded at 320 K, significantly higher than room temperature. This observation implies that the entire workpiece is influenced by the intense heat generated by this shoulder size compared to smaller sizes. Additionally, the figure shows a notable increase in the area covered by temperature contours from a to d, highlighting the substantial effect of shoulder size on thermal distribution.



**Figure 6:** Static temperature contours for different shoulder diameters a=26mm, b=34mm, c=42mm, d=50mm.

#### 4. CONCLUSION

In conclusion, this study highlights the significant influence of shoulder size on the temperature distribution and thermal characteristics in friction stir welding. Through simulations, it was observed that larger shoulder diameters result in higher peak temperatures and an expanded thermal impact zone within the workpiece. The highest temperatures were consistently recorded near the shoulder-workpiece interface, indicating that frictional heating at this contact area is the primary heat source in FSW. Additionally, the temperature gradient displayed a steeper increase ahead of the tool than behind it, due to reduced thermal diffusivity and heat accumulation in the trailing region. This asymmetry in heat distribution suggests that shoulder size not only affects the peak temperature but also influences the temperature dissipation rate across the workpiece. The findings underscore that optimizing shoulder size is essential for controlling the thermal profile and, consequently, the mechanical properties of FSW joints, providing valuable insights for enhancing welding parameters and joint performance.

#### 5. REFERENCES

- [1] Christy, JV, & Ismail Mourad, AH. "Friction Stir Welding of Hybrid Recycled Metal Matrix Composites." Proceedings of the . Volume 4A: Materials and Fabrication. Las Vegas, Nevada, USA. July 17–22, 2022. V04AT06A046. ASME. <https://doi.org/10.1115/PVP2022-84429>
- [2] Chenghang Zhang, Guangjie Huang, Yu Cao, Yulong Zhu, Qing Liu, On the microstructure and mechanical properties of similar and dissimilar AA7075 and AA2024 friction stir welding joints: Effect of rotational speed, Journal of Manufacturing Processes, Volume 37, 2019, Pages 470-487, ISSN 1526-6125, <https://doi.org/10.1016/j.jmapro.2018.12.014>.
- [3] Kah P, Martikainen J. Current trends in welding processes and materials: improve in effectiveness. Rev. adv. mater. Sci. 2012 Apr 1;30(2):189-200.
- [4] P. Balasundar, S. Senthil, P. Narayanasamy, Peerawatt Nunthavarawong, Abhilashsharan Tambak, T. Ramkumar, B.K. Parrthipan, Tribo-mechanical performance of Al-nano TiC composites processed by microwave-assisted powder metallurgy, Ceramics International, Volume 50, Issue 19, Part B, 2024, Pages 36448-36457, ISSN 0272-8842, <https://doi.org/10.1016/j.ceramint.2024.07.030>.

- 
- [5] Chenghang Zhang, Yu Cao, Guangjie Huang, Qinghui Zeng, Yulong Zhu, Xinde Huang, Na Li, Qing Liu, Influence of tool rotational speed on local microstructure, mechanical and corrosion behavior of dissimilar AA2024/7075 joints fabricated by friction stir welding, *Journal of Manufacturing Processes*, Volume 49, 2020, Pages 214-226, ISSN 1526-6125, <https://doi.org/10.1016/j.jmapro.2019.11.031>.
- [6] Y.C. Chen, J.C. Feng, H.J. Liu, Precipitate evolution in friction stir welding of 2219-T6 aluminum alloys, *Materials Characterization*, Volume 60, Issue 6, 2009, Pages 476-481, ISSN 1044-5803, <https://doi.org/10.1016/j.matchar.2008.12.002>.
- [7] Sufian Raja, Mohd Ridha Muhamad, Mohd Fadzil Jamaludin, Farazila Yusof, A review on nanomaterials reinforcement in friction stir welding, *Journal of Materials Research and Technology*, Volume 9, Issue 6, 2020, Pages 16459-16487, ISSN 2238-7854, <https://doi.org/10.1016/j.jmrt.2020.11.072>.
- [8] Jianing Li, Molin Su, Wenjun Qi, Chen Wang, Peng Zhao, Fei Ni, Kegao Liu, Mechanical property and characterization of 7A04-T6 aluminum alloys bonded by friction stir welding, *Journal of Manufacturing Processes*, Volume 52, 2020, Pages 263-269, ISSN 1526-6125, <https://doi.org/10.1016/j.jmapro.2020.02.018>.
- [9] R.S. Mishra, Z.Y. Ma, Friction stir welding and processing, *Materials Science and Engineering: R: Reports*, Volume 50, Issues 1–2, 2005, Pages 1-78, ISSN 0927-796X, <https://doi.org/10.1016/j.mser.2005.07.001>.
- [10] Rahul Kesharwani, Kishor Kumar Jha, Murshid Imam, Chiranjit Sarkar, Imad Barsoum, Comparison of microstructural, texture and mechanical properties of SiC and Zn particle reinforced FSW 6061-T6 aluminium alloy, *Journal of Materials Research and Technology*, Volume 26, 2023, Pages 3301-3321, ISSN 2238-7854, <https://doi.org/10.1016/j.jmrt.2023.08.161>.